

# Development and Validation of a Practical Lower-Dose-Simulation Tool for Optimizing Computed Tomography Scan Protocols

Lifeng Yu, PhD, Maria Shiung, BA, Dayna Jondal, BA, and Cynthia H. McCollough, PhD

**Objective:** The objective of this study was to develop and validate a novel noise insertion method that can accurately simulate lower-dose images from existing standard-dose computed tomography (CT) data.

**Methods:** The noise insertion method incorporates the effects of the bowtie filter, automatic exposure control, and electronic noise. We validated this tool using both phantom and patient studies. The phantom study compared simulated lower-dose images with the actually acquired lower-dose images. The patient studies included 105 pediatric and 24 adult CT body examinations.

**Results:** The noise level in the simulated images was within 3.2% of the actual lower-dose images in phantom experiments. Noise power spectrum also demonstrated excellent agreement. For the patient examinations, a mean difference of noise level between 2.0% and 9.7% was observed for simulated dose levels between 75% and 30% of the original dose.

**Conclusions:** An accurate technique for simulating lower-dose CT images was developed and validated, which can be used to retrospectively optimize CT protocols.

**Key Words:** computed tomography (CT), radiation dose reduction, protocol optimization

(*J Comput Assist Tomogr* 2012;36: 477–487)

The increased use of computed tomography (CT) imaging has generated concerns regarding the potential cancer risks associated with the radiation exposure from CT.<sup>1</sup> Optimizing CT protocols to achieve adequate diagnostic performance with the lowest acceptable dose has therefore become an essential task.<sup>2,3</sup> Despite the tremendous efforts of the CT community to minimize radiation dose,<sup>4</sup> scan protocols and radiation doses still vary widely among different CT practices.<sup>5,6</sup> This is largely attributable to the lack of an efficient and widely available approach to optimizing CT protocols.

Clinical evaluation by interpreting physicians is the most commonly used approach to determining the lowest possible radiation dose in CT protocols.<sup>7–9</sup> One method of evaluation is to gradually decrease the scanner radiation output until the image quality approaches the minimum acceptable limit. This approach requires exploratory lower-dose scans on a number of patients, which is tedious and can potentially result in a diagnostically compromised image. A more elegant approach is to use a noise insertion tool to simulate images at reduced dose levels from existing “standard dose” examinations. A range of simulated dose levels can be generated, and diagnostic quality comparisons

can be made within the same patient, removing patient-specific variables and allowing assessment of clinically relevant findings.<sup>8,10–13</sup> Because of the proprietary nature of the CT raw data format, the noise insertion tools for clinical use have often been developed by manufacturers of CT scanners and distributed to very few users under research agreements. The technical details of the tools are not fully described in the literature, which makes their applications rather limited.

In this work, we describe a simple noise insertion method that can accurately simulate both the noise level and spatial frequency content of lower-dose images from existing standard-dose CT data. This noise insertion method takes into account several important physical traits of a CT scanner that can substantially affect noise characteristics, including the x-ray beam bowtie filter, automatic exposure control (AEC), and electronic noise. We validated this technique in phantom studies by comparing the noise level and noise power spectrum (NPS) in the simulated lower-dose images with images acquired at the corresponding actual dose levels. We also validated the technique in 105 pediatric patients and 24 adult patients by comparing the noise level measured in simulated lower-dose images to that theoretically predicted from the standard-dose patient images.

## MATERIALS AND METHODS

### CT Noise Model

Noise in CT images originates from noise in the original projection measurement, which has 2 principal sources: quantum noise and electronic noise.<sup>14</sup> Although modern CT detectors are not photon-counting elements, but rather energy integrators, a photon-counting model is still a good approximation of quantum noise and is widely used for characterizing CT noise.<sup>15–19</sup> More accurate noise models, such as compound Poisson model, were proposed.<sup>20</sup> As explained by Whiting et al,<sup>20</sup> the bowtie filter and tube current modulation have a greater effect on the noise characteristics of CT data than the noise model itself. Therefore, for simplicity, we used a photon-counting model in this work and considered the effect of bowtie filter and tube current modulation.

For a given path of an x-ray photon through the imaged subject, the incident and the penetrated photon numbers were denoted  $N_0(k, l, m)$  and  $N(k, l, m)$ , respectively, where  $k$  and  $l$  denote the index of detector bins along axial and longitudinal directions, respectively, and  $m$  the index of projection angle. In the presence of quantum noise, the measured data should be considered as a stochastic process. Ideally, the line integral along the attenuating path is given by

$$P_i = -\ln(N_i/N_{0i}). \quad (1)$$

Herein, for expression simplicity, we use a single discrete index  $i$  to represent the data index  $(k, l, m)$ . We use a bold letter and the corresponding normal letter to denote a stochastic process and

From the Department of Radiology, Mayo Clinic, Rochester, MN. Received for publication February 9, 2012; accepted April 4, 2012. Reprints: Lifeng Yu, PhD, 200 First St SW, Rochester, MN 55905 (e-mail: yu.lifeng@mayo.edu).

This work was supported in part by a research grant from Thrasher Research Foundation.

The authors have no conflict of interest to report. Copyright © 2012 by Lippincott Williams & Wilkins

its mean, respectively. Assuming that data collected in each detector bin are uncorrelated, it can be shown that, to a very good approximation,<sup>15</sup> the mean of  $\mathbf{P}_i$  is  $-\ln(N_i / N_{0i})$  and the covariance of  $\mathbf{P}_i$  is given by

$$\text{Cov}\{\mathbf{P}_i, \mathbf{P}_{i'}\} = \frac{1}{N_i} \delta_{ii'} = \frac{\exp(P_i)}{N_{0i}} \delta_{ii'} \quad (2)$$

where  $\delta_{ii'}$  denotes the Kronecker delta function. This model is similar to the noise model obtained by Li and colleagues from repeated measurements on a CT scanner.<sup>16,17</sup>

### Noise Insertion Algorithm

For a given tube potential and detector collimation, the data acquired with the original tube current setting can be expressed as  $\mathbf{P}_A = -\ln(N_A / N_{0A})$ , where  $N_{0A}$  and  $N_A$  are the incident and penetrated number of photons, respectively, along a given ray path indexed by  $i$ , and  $N_{0A}$  is proportional to the value of the tube current setting, expressed as tube current (mA), tube current time product (mAs), or effective mAs (mAs/pitch). Herein, we neglect the index  $i$  for simplicity. Under typical clinical conditions, the detected number of photons  $N_A$  exceeds 20, and the measured data can thus be considered normally distributed,<sup>20</sup> which can be expressed as

$$\mathbf{P}_A = P + \frac{1}{\sqrt{N_A}} \mathbf{x} = P + \frac{1}{\sqrt{N_{0A} \exp(-P)}} \mathbf{x}, \quad (3)$$

where  $P$  is the mean value of the data, and  $\mathbf{x}$  is a normally distributed stochastic process with a zero mean and a unit variance. If the tube current setting is reduced to a lower level with a scaling factor of  $a$ ,  $0 < a < 1$ , the corresponding incident number of photons is  $N_{0B} = aN_{0A}$ , and the measured data can be expressed as

$$\mathbf{P}_B = P + \frac{1}{\sqrt{N_B}} \cdot \mathbf{x} = P + \frac{1}{\sqrt{aN_{0A} \exp(-P)}} \cdot \mathbf{x}. \quad (4)$$

It should be noted that the true value of  $P$  is unknown, so  $\mathbf{P}_B$  is also unknown without a direct measurement. However, if the data  $\mathbf{P}_A$  measured at a higher tube current setting is available, then one can obtain an approximation of  $\mathbf{P}_B$  by adding noise to  $\mathbf{P}_A$ . The level of noise added will have to make the simulated data  $\tilde{\mathbf{P}}_B$  have the same mean and SD as  $\mathbf{P}_B$ . The following expression satisfies this requirement:

$$\begin{aligned} \tilde{\mathbf{P}}_B &= \mathbf{P}_A + \sqrt{\frac{1}{N_B} - \frac{1}{N_A}} \cdot \mathbf{x} \\ &= \mathbf{P}_A + \sqrt{\left(\frac{1}{N_{0B}} - \frac{1}{N_{0A}}\right) \cdot \exp(P)} \cdot \mathbf{x}. \end{aligned} \quad (5)$$

Because  $\mathbf{P}_A$  is acquired with a higher tube current setting, one can use  $\mathbf{P}_A$  to approximately represent the true value  $P$ , and Eq. (5) can be approximately expressed as

$$\begin{aligned} \tilde{\mathbf{P}}_B &\approx \mathbf{P}_A + \sqrt{\left(\frac{1}{N_{0B}} - \frac{1}{N_{0A}}\right) \cdot \exp(P_A)} \cdot \mathbf{x} \\ &= \mathbf{P}_A + \sqrt{\frac{1-a}{a} \cdot \frac{\exp(P_A)}{N_{0A}}} \cdot \mathbf{x}. \end{aligned} \quad (6)$$

### Quantifying the Incident Number of Photons

As can be seen from Eq. (6), in order to simulate CT data with a reduced mAs setting from existing data acquired with a higher mAs setting ( $N_{0B} = aN_{0A}$ ,  $0 < a < 1$ ), one has to determine the incident number of photons,  $N_{0A}$ , in the existing data along each ray path. The incident number of photons can be expressed in terms of the number of photons that provides the same noise as in the existing data, assuming a quantum limit condition. This method is suggested by Whiting et al<sup>20</sup> to estimate the noise-equivalent quanta. The variance of the transmission data is given by

$$\text{var}\{\exp(-\mathbf{P})\} = \text{var}\left\{\frac{N}{N_0}\right\} \approx \frac{N}{N_0^2}. \quad (7)$$

Therefore, for an air scan, the variance of the transmission data is given by

$$\text{var}\{\exp(-\mathbf{P}_{air})\} = \frac{1}{N_0}. \quad (8)$$

One can perform an air scan and calculate the variance of the transmission data to obtain the noise-equivalent quanta at a given mAs level. The incident number of photons at other mAs levels can be readily derived based on this calibration.

At each angle, the x-ray projection covers a 2-dimensional (2D) detector area. Along each detector row, the use of the bowtie filter changes the incident number of photons. In addition, tube current modulation is often used, which changes the incident number of photons for different projection angles. Therefore, to quantify the incident number of photons, one needs to incorporate both of these effects.

### Incorporation of the Effect of X-ray Beam Bowtie Filter

A bowtie filter is often used in clinical CT scanners to reduce the incident x-ray intensity to the patient periphery so that the radiation dose to the patient, especially the skin dose, can be minimized. As a consequence, the x-ray intensity incident to the patient is highly nonuniform across the fan beam, which will affect the noise properties in the measured CT data. The effect of the bowtie filter can be quantified by measuring the variance of the transmission from an air scan (without any attenuating object inside the field of view). The inverse of the variance is the noise-equivalent quanta, which can be used to estimate the incident number of photons across the x-ray beam, as given by Eq. (8).

### Incorporation of the Effect of AEC

Automatic exposure control is widely used for dose reduction in CT. Figure 1 shows an example of AEC in a chest/abdomen/pelvis examination. A commercially available AEC system (CAREDose4D; Siemens Healthcare, Forchheim, Germany) was used during the examination. The white curve represents the tube current as a function of table position. The tube current is modulated during the gantry rotation to adapt the radiation output to the attenuation of the patient at different projection angles. This automatic tube current modulation leads to substantial changes in the incident x-ray intensity, which will also affect the noise characteristics of the CT data. This effect can be incorporated into the noise insertion algorithm by extracting the reference signal from each projection frame, which is available from the CT raw data and then estimating the corresponding incident number of photons. The calibration curves determined from the bowtie filter can be used for this estimation.

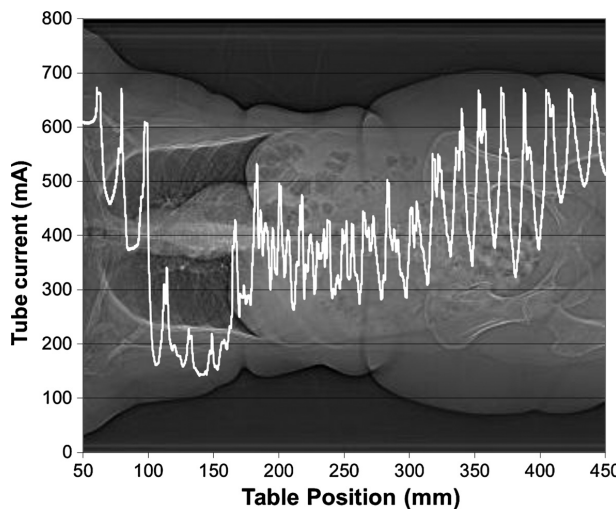


**FIGURE 1.** Effect of AEC on tube current. An example of AEC in a chest/abdomen/pelvis patient examination is shown. The white curve represents tube current as a function of table position. The tube current oscillates as the table translates to adapt to the different attenuation levels of the patient along different projection angles.

### Incorporation of Electronic Noise

When the detected number of photons is low, the electronic noise cannot be neglected. A typical way to express the electronic noise is to assume that the variance of the detected number of photons follows that described in the study of Hsieh<sup>21</sup>:

$$\text{var}\{N\} = \sigma_e^2 + \sigma_q^2 = N_e + N, \quad (9)$$

where  $\sigma_q$  represents the quantum noise, and  $\sigma_e$  represents the SD of the electronic noise floor of the detection system (the noise-equivalent quanta of this noise floor is given by  $N_e = \sigma_e^2$ ). Therefore, to the first-order approximation, the variance of data  $P$  can be expressed as

$$\text{var}\{P\} = \text{var}\left\{\ln \frac{N_0}{N}\right\} \approx \frac{N_e + N}{N^2}. \quad (10)$$

Using Eq. (10), it can be shown that the data to approximate  $P_B$  by adding noise can be approximately expressed as

$$\tilde{P}_B \approx P_A + \sqrt{\frac{1-a}{a} \cdot \exp(P_A)} \cdot \left(1 + \frac{1+a}{a} \cdot \frac{N_e \cdot \exp(P_A)}{N_{0A}}\right) x. \quad (11)$$

In a typical clinical setting and for simulation of a dose that is not extremely low, the impact of electronic noise is negligible. For example, when scanning an average-size patient with a lateral width of 36 cm using a technique of 120 kV and 240 mAs, the number of detected photons in terms of noise-equivalent quanta is about  $1.4 \times 10^5$  per detector reading, and the detected number of photons is  $1.4 \times 10^5 \times \exp(-0.2 \text{ cm}^{-1} \times 36 \text{ cm}) = 104$ . In a simulation of a 50% mAs level from the original 240 mAs, the detected number of photons is 52, which is still much higher than the electronic noise floor. Assuming  $N_e = 5$ , the electronic noise term contributes only about 6% of the overall noise. Only when the simulated mAs level is very low and the detected number of photons approaches the electronic noise floor does the electronic noise term have a meaningful impact on the image noise. For example, if simulating a 30-mAs level from the original 240-mAs data for the same patient, the detected

number of photons would be only about 12. In this situation, the contribution from electronic noise cannot be neglected.

In this study, we used the following calibration method to estimate  $N_e$ . A cylindrical water phantom with a diameter of 30 cm was scanned at 4 effective mAs levels (240, 120, 60, and 30). Noise was introduced to the raw data acquired at 240 mAs based on Eq. (11) to simulate the 3 lower mAs levels. Different values of  $N_e$  (0, 5, 10, and 15) were used to simulate images at each mAs level. Noise was measured from each acquired image and each simulated image. The difference in image noise between the actually scanned images and the simulated images was plotted as a function of the assumed electronic noise value and a linear regression performed. Extrapolation of the regression equation was performed to determine the electronic noise value that best corresponded to a difference of zero between the noise values measured in the actual and simulated images.

### Validation of the Noise Insertion Tool Using Phantom Studies

#### Pediatric Body CT

We evaluated the noise insertion tool in pediatric body CT by using a series of acrylic cylindrical phantoms (8.7, 10.1, 12.7, and 14 cm in diameter; Fig. 2A) simulating the attenuation level of a newborn, 4-month-old infant, 1-year-old, and 2-year-old, respectively. For each phantom, CT scans were acquired on a dual-source 64-slice scanner (Definition; Siemens Healthcare) with an effective mAs of 80, 40, and 20; a tube potential of 120 kV; a rotation time of 0.33 seconds; a detector collimation of  $64 \times 0.6$  mm; and a helical pitch of 0.5. Automatic exposure control was off for these scans. After exporting the projection data from the 80-mAs scan to an off-line computer, lower-dose projection data at 40 and 20 mAs settings were simulated according to the described methods. The simulated raw data were placed into the manufacturer's raw data file format and returned to the scanner for image reconstruction using exactly the same parameters: B40, 3-mm slice thickness, and 3-mm interval. The noise level was measured in 5 regions of interest (ROIs) per image in both the simulated and acquired lower-dose images. The noise measurement was averaged over 10 contiguous images along longitudinal direction for each of the 4 cylindrical phantoms.

#### Adult Body CT

To examine the method in the presence of more complex anatomical structures, an adult anthropomorphic phantom was evaluated (Fig. 2B). The phantom was scanned on a dual-source 128-slice scanner (Definition Flash; Siemens Healthcare). The

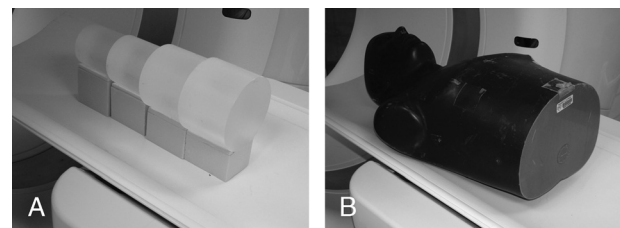


**FIGURE 2.** Phantoms used for validating the accuracy of the noise insertion tool. A, A series of acrylic cylindrical phantoms with diameters of 8.7, 10.1, 12.7, and 14 cm representing the attenuation level of a newborn, 4-month-old infant, 1-year-old child, and 2-year-old child. B, An anthropomorphic phantom representing an adult patient.

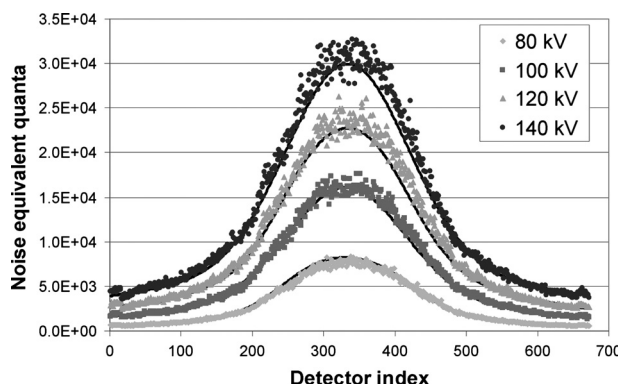


**FIGURE 3.** Noise-equivalent quanta as a function of detector index along a single detector row for different tube potentials at 80, 100, 120, and 140 kV. The nonuniform noise-equivalent quanta are a result of x-ray beam bowtie filter.

scanning parameters were as follows: 120 kV, quality reference mAs (QRM) = 240, 128 × 0.6-mm collimation, rotation time of 0.5 second, and helical pitch of 0.6. Automatic exposure control was on (CARE Dose4D, Siemens Healthcare). All scans were from top of the shoulder to the upper abdomen. Images were reconstructed using a B40 kernel with a slice thickness of 5 mm and a reconstruction interval of 5 mm. In addition to the scan at a QRM of 240, 3 additional scans were performed with QRM settings of 120, 60, and 30. Lower-dose images at 120, 60, and 30 QRM settings were simulated according to the described methods. Noise was measured every 4 cm from top of the shoulder to the abdomen on both acquired and simulated images. Three ROIs were measured per reconstructed image, and the mean noise per image calculated. Exactly the same ROI locations were used for noise measurements in both acquired and simulated images. The noise level in the simulated lower-dose images was compared with images acquired at the corresponding actual lower-dose levels.

### Adult Head CT

Using the same adult anthropomorphic phantom (Fig. 2B), we validated the noise insertion tool in head CT examinations. The head of the phantom was scanned on a dual-source 128-slice scanner (Definition Flash; Siemens Healthcare). The scanning

parameters were as follows: 120 kV, effective mAs of 400, 128 × 0.6-mm collimation, rotation time of 1.0 second, and helical pitch of 0.6. Automatic exposure control was off. Images were reconstructed using an H41 kernel with a slice thickness of 5 mm and a reconstruction interval of 5 mm. Three additional scans were performed with effective mAs settings of 200, 100, and 50. Lower-dose images at 200, 100, and 50 effective mAs settings were simulated from the full-dose data. Noise was measured on 5 contiguous images at each dose level. Five ROIs were measured per image, and the mean noise at each dose level calculated. The noise level in the simulated lower-dose images was compared with images acquired at the corresponding actual lower-dose levels.

### Validation Using NPS

Image noise, quantified using the SD of CT numbers in a uniform ROI, represents only the first-order noise properties of an image. Diagnostic performance is also critically dependent on the spatial frequency distribution of the noise. The NPS is a more complete representation of the noise properties of the image.<sup>22–24</sup> In addition to validation using the noise level (SD), we also calculated and compared the 2D NPS in the simulated and acquired lower-dose images using scans of a 30-cm-diameter water phantom. The scanning parameters were as follows: 120 kV, 128 × 0.6-mm collimation, rotation time of 0.5 second, and helical pitch of 0.6. Automatic exposure control was off. Three dose levels were acquired with an effective mAs of 240, 120, and 60, respectively. Images were reconstructed using a B40 kernel with a slice thickness of 5 mm and a reconstruction interval of 5 mm. The 240-mAs data were used to simulate 120- and 60-mAs data. The calculation of the 2D NPS followed that in the study of Boedeker et al<sup>23</sup> and was averaged over 11 images for each dose level. A 1-dimensional NPS profile was calculated by circularly averaging the 2D NPS.

### Validation of the Noise Insertion Tool Using Patient Examinations

Under an institutional research board-approved protocol, we collected raw projection data from clinically indicated scans of the chest, abdomen, and pelvis in 24 adults and 105 children. All adult scans were acquired using 120 kV and a QRM of 240 (AEC was on). The pediatric scans were acquired following a weight-based kV/mAs technique chart<sup>25</sup> including 26 cases at 80 kV, 40 cases at 100 kV, and 39 cases at 120 kV. For each

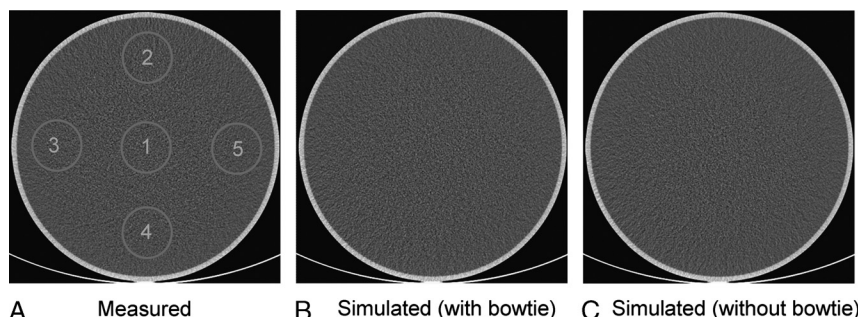


**FIGURE 4.** Impact of bowtie filter on noise distribution in simulated images. A, An actually acquired image obtained with 120 effective mAs on a cylindrical water phantom. The 5 circles are ROIs where noise was measured. B, Simulated image at 120 effective mAs incorporating the effect of the bowtie filter. C, Simulated image at 120 effective mAs without incorporating the effect of the bowtie filter. Both simulations were obtained by inserting noise into the raw data acquired at 240 effective mAs. The noise comparison for the 5 ROIs is shown in Table 1. The simulated image without the bowtie filter has the same noise level in the center ROI, but the noise estimates in peripheral ROIs were 7% lower than in the acquired image. The simulated image with bowtie filter has the same noise level as the acquired image in both center and peripheral ROIs.

**TABLE 1.** Impact of Bowtie Filter on Noise Distribution in Simulated Images

ROI	Measured		Simulated (Bowtie)		Simulated (No Bowtie)	
	Noise Level, HU	SD, HU	Noise Level, HU	SD, HU	Noise Level, HU	SD, HU
1	20.1	0.3	19.9	0.2	19.8	0.2
2	16.2	0.8	16.3	0.9	15.1	0.9
3	16.6	0.9	16.3	0.6	15.0	0.7
4	17.6	0.7	17.5	1.1	15.9	0.9
5	16.8	0.8	16.8	0.7	15.4	0.7
Mean	17.4	0.7	17.4	0.7	16.2	0.7

Noise level at each ROI was obtained by averaging the SD of each ROI over 10 contiguous slices. Locations of ROIs for noise measurement are displayed in Figure 4A.

examination, we simulated 3 additional dose levels (75%, 50%, and 25% of the original dose for adults and 70%, 50%, and 30% of the original dose for children). These simulated lower-dose images were used to determine the lowest-acceptable dose levels and to optimize the scanning protocols. As the first step of these evaluations, a validation of the noise insertion was performed. Noise was measured on images obtained at all 4 dose levels using exactly the same 3 ROIs within each patient, and the average noise level calculated. The noise level measured on the simulated images was compared with theoretical noise levels, which were estimated from the full-dose image according to the inverse square root relationship between noise and dose. This method was also used in the study of Ciaschini et al<sup>13</sup> because the actual values that would have been obtained with lower dose levels in patients were not known.

## RESULTS

### Calibration of the Incident Number of Photons

Figure 3 shows the noise-equivalent quanta calculated as the inverse of the variance of the transmission data (Eq. 8) and plotted as a function of detector bin along a single detector row. The transmission data were obtained from air scans performed

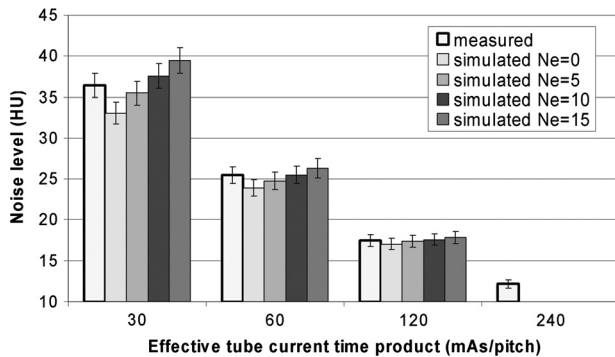


**FIGURE 5.** Calibration of electronic noise using a cylindrical water phantom with a diameter of 30 cm. Bar plots of noise levels averaged over 50 ROIs (5 ROIs in 10 contiguous slices) are shown to compare noise in acquired images and simulated images when different electronic noise was used in the simulation. Noise was inserted into the data acquired at 240 mAs to simulate 120, 60, and 30 mAs, assuming the electronic noise  $N_e = 0, 5, 10$ , and 15.

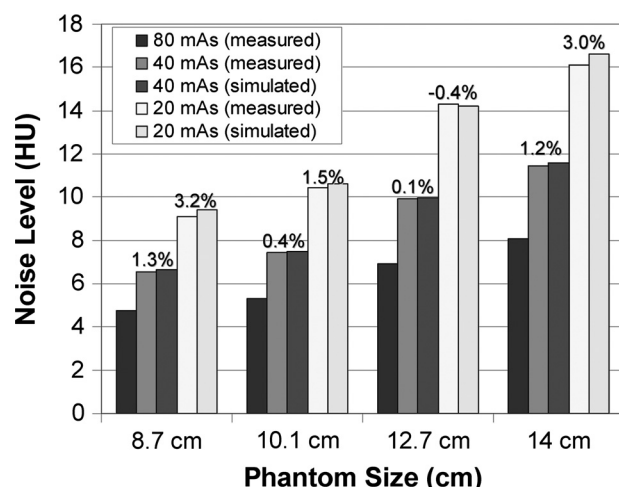


**FIGURE 6.** Validation of the noise insertion tool using a series of acrylic cylindrical phantoms with diameters of 8.7, 10.1, 12.7, and 14 cm representing the attenuation level of a newborn, 4-month-old infant, 1-year-old child, and 2-year-old child, respectively. Noise levels were compared between simulated and acquired images at 2 different mAs levels. The noise insertion tool was used to simulate images from raw data acquired at an effective mAs of 80.

at different tube potentials (80, 100, 120, and 140 kV) at a mAs level of 40. It can be seen that the incident number of photons decreased by a factor of approximately 8 from the center to the peripheral region of the x-ray beam. For any other mAs level, these curves can be scaled to obtain the incident number of photons used in the noise insertion tool.

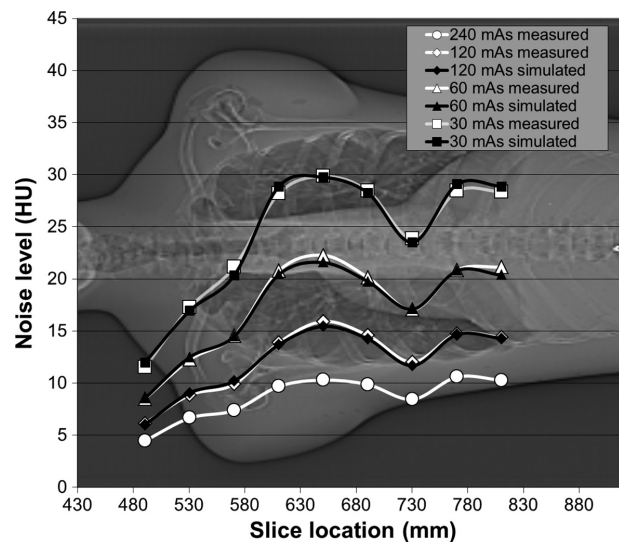


**FIGURE 7.** Validation of the noise insertion tool using an anthropomorphic phantom representing an adult patient. Noise levels were compared between simulated images and acquired images at 3 different mAs levels. The simulated images were generated from the raw data acquired at a QRM of 240 using the noise insertion tool. The AEC was turned on. The plots are overlaid on a CT radiograph, indicating the location of each slice where noise was measured. The noise changes at different slice locations but is similar for the acquired and simulated images at each slice.

## Impact of a Bowtie Filter on Noise Distribution in Simulated Images

The effect of the nonuniform incident number of photons across the x-ray beam as a result of the bowtie filter on the simulated image noise is illustrated in Figure 4: Figure 4A is an actual image acquired with 120 effective mAs on a cylindrical water phantom, and Figures 4B and C are simulated images at 120 effective mAs with and without incorporating the effect of the bowtie filter, respectively. Both simulations were obtained by inserting noise into the raw data acquired at 240 effective mAs. When we compared noise levels measured at 5 different ROIs (Fig. 4A, each averaged over 10 contiguous slices) among these images, the simulated image without bowtie filter had the same noise level in the center ROI as the acquired image, but the estimated noise in peripheral ROIs was 7% lower than in the acquired image (Table 1). The simulated image with the bowtie filter had a similar noise level as the acquired image in both center and peripheral ROIs.

## Calibration of Electronic Noise

Estimation of the electronic noise level by comparing measured versus simulated noise levels for different levels of assumed electronic noise resulted in values of 7.3, 9.7, and 7.6 at mAs levels of 120, 60, and 30, respectively (Fig. 5). An averaged value of 8.2 was obtained and used in the simulation.

## Validation of the Developed Noise Insertion Tool Using Phantom Studies

### Pediatric Body CT

As shown in Figure 6, the percent differences in noise level between the simulated and acquired lower-dose images were 3.2% or less for all 4 phantom sizes.

### Adult Body CT

Using an anthropomorphic adult phantom and scans acquired using AEC, the noise measured on the simulated images

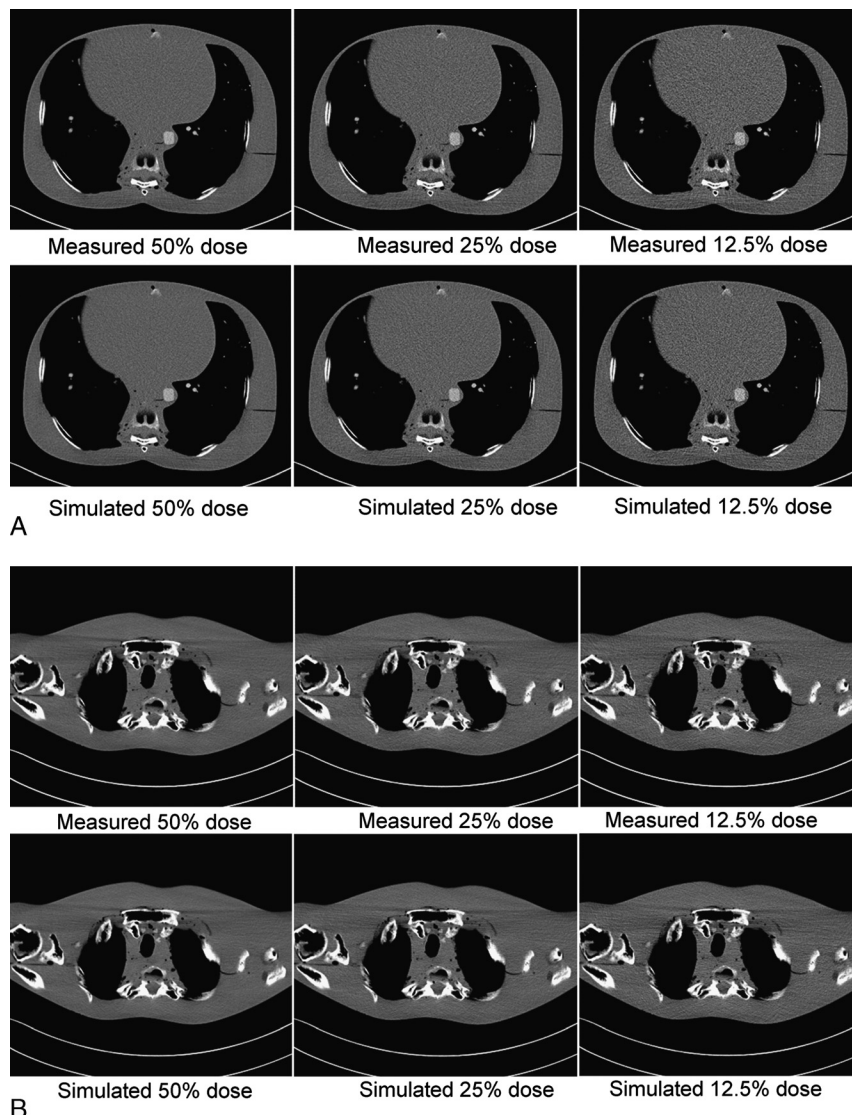


**FIGURE 8.** Comparison between simulated images and acquired images at different dose levels on an anthropomorphic phantom. Two slice locations are shown: (a) chest and (b) shoulder. The original dose level corresponds to a QRM of 240. Display window/level = 400/40 Hounsfield Unit (HU).

**TABLE 2.** Validation of the Noise Insertion Tool in Head Scans Using Phantoms

	<b>Full Dose</b>	<b>50% Dose</b>		<b>25% Dose</b>		<b>12.5% Dose</b>	
	<b>Measured Noise, HU</b>	<b>Measured Noise, HU</b>	<b>Simulated Noise, HU</b>	<b>Measured Noise, HU</b>	<b>Simulated Noise, HU</b>	<b>Measured Noise, HU</b>	<b>Simulated Noise, HU</b>
ROI 1	4.7	6.7	6.6	9.6	9.4	14.0	13.1
ROI 2	4.7	6.7	6.5	9.4	8.9	13.5	12.8
ROI 3	4.7	6.3	6.5	9.0	9.0	13.1	12.7
ROI 4	4.7	6.6	6.6	9.0	9.2	12.9	13.6
ROI 5	4.6	6.4	6.3	8.7	8.7	13.0	12.5
Average	4.7	6.5	6.5	9.1	9.0	13.3	13.0
Percent difference	NA		-0.9%		-0.8%		-2.6%

Noise in each ROI was measured and averaged over 5 contiguous images. The full-dose technique corresponds to 400 effective mAs.

NA indicates not applicable.

agreed with that measured on the acquired images at each dose level and image location (Fig. 7). The mean percent error in noise level was 2.0% (SD, 1.5%), 1.9% (SD, 1.0%), and 2.1% (SD, 1.3%) for the simulated images at 50%, 25%, and 12.5% dose levels, respectively. In addition to the agreement in noise level, the noise texture also appeared visually similar at all dose levels (Figs. 8A, B).

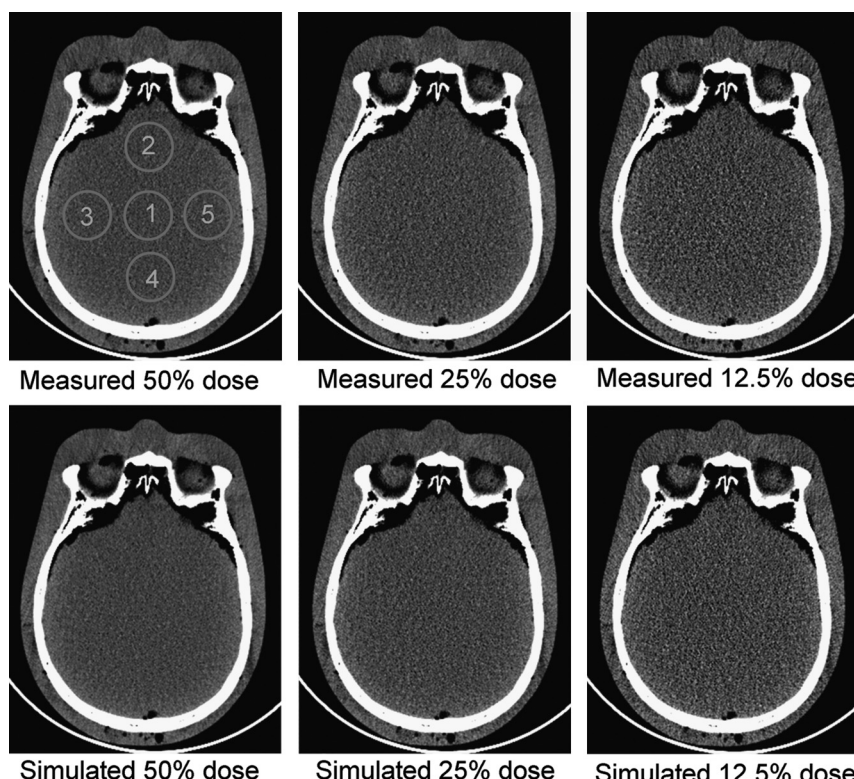
#### Adult Head CT

Table 2 compares the noise level of the simulated and acquired lower-dose images using the head phantom; the percent differences were 2.6% or below. Figure 9 shows an example of

images comparing simulated and acquired lower-dose images at 50%, 25%, and 12.5% dose levels. The 5 ROIs used for noise comparison were shown in the acquired 50% dose image.

#### Noise Power Spectra

In both simulated lower-dose images and measured lower-dose images, the peak noise power occurred at a spatial frequency of about 2.8 line pairs/cm (Fig. 10). The shape and magnitude of the NPS from the simulated 50% and 25% dose images matched those from the measured 50% and 25% dose images very closely.



**FIGURE 9.** Comparison between simulated images and acquired images at different mAs levels on an anthropomorphic head phantom. The original dose level corresponds to an effective mAs of 400. Display window/level = 120/40 HU.

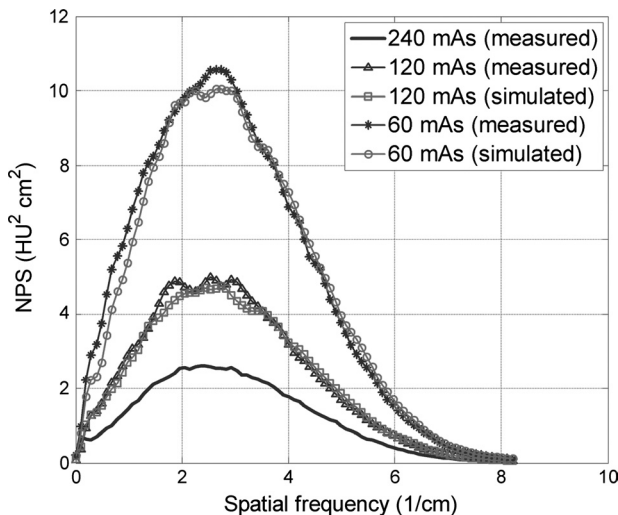


**FIGURE 10.** Comparison of the NPS on simulated images and acquired images at 2 different mAs levels. The NPS on the 80-mAs images is displayed as a reference.

### Validation of the Noise Insertion Tool Using Patient Cases

We measured noise in simulated images and predicted the theoretical noise level at each dose level for 105 pediatric body examinations (Table 3) and 24 adult chest/abdomen/pelvic examinations (Table 4). The noise difference increased with the decrease in the simulated dose level (pediatric CT: 3.7% for 50% dose level and 5.4% for 30% dose level; adult CT: 4.6% for 50% dose level and 9.7% for 25% dose level). Figures 11 and 12 show 2 examples of lower-dose simulated images, one from an adult chest examination and the other from a pediatric abdominal examination. The higher percentage differences observed in patient cases than in phantom studies were probably due to the lack of measured noise level in lower-dose patient examinations. The inverse square root relation between noise and mAs was used to generate the “true” noise values at lower-dose levels, which may have a small bias, especially when the simulated mAs level is low, and the influence of electronic noise increases. Considering the excellent agreement in phantom studies, where actual lower-dose images were acquired and compared with simulated lower-dose

**TABLE 4.** Validation of the Noise Insertion Tool in 24 Adult Abdominal Examinations

mAs level*	75%	50%	25%
Mean difference†	2.0%	4.6%	9.7%
SD‡	1.7%	3.4%	9.2%

\*The mAs level is relative to that used in the original examination, which was 240 QRM for all adult patients.

†The mean difference was calculated as the percentage difference between the noise level in simulated images and the theoretically predicted noise level. The value was averaged over the 24 patients. The theoretical prediction at each mAs level was based on the inverse square root relation between noise and mAs level.

‡The SD was calculated from the noise difference over the 24 adult patients.

images, and because the inverse square root relationship does not take into account the complex effects of the electronic noise, we consider a difference within 10% in patient examinations to be adequate for use in optimizing clinical examination protocols.

### DISCUSSION

Our noise insertion tool can simulate lower-dose examinations from existing “standard dose” examinations, thus enabling radiologists to determine the lowest acceptable dose level without having to re-expose the patient and without the risk of compromising a patient scan when testing a lower-dose technique. Many investigators have used noise insertion tools to optimize CT scanning protocols for examination types including chest CT,<sup>10</sup> CT colonography,<sup>11</sup> pediatric abdominal CT,<sup>12</sup> and CT for urinary stone detection.<sup>13</sup> However, the noise insertion tools used in these studies were all provided by the scanner manufacturers. Although the accuracy of the tools was usually validated as a part of each study, the technical details of the

**TABLE 3.** Validation of the Noise Insertion Tool in 105 Pediatric Body CT Examinations

mAs level*	70%	50%	30%
Mean difference†	2.6%	3.7%	5.4%
SD‡	2.5%	3.3%	4.4%

\*The mAs level is relative to that used in the original examination, which was 50 QRM for abdominal examinations and 40 QRM for chest examinations.

†The mean difference was calculated as the percentage difference between the noise level in simulated images and theoretically predicted noise level. The value was averaged over the 105 patients. The theoretical prediction at each mAs level was based on the inverse square root relation between noise and mAs level.

‡The SD was calculated from the noise difference over the 105 pediatric patients.

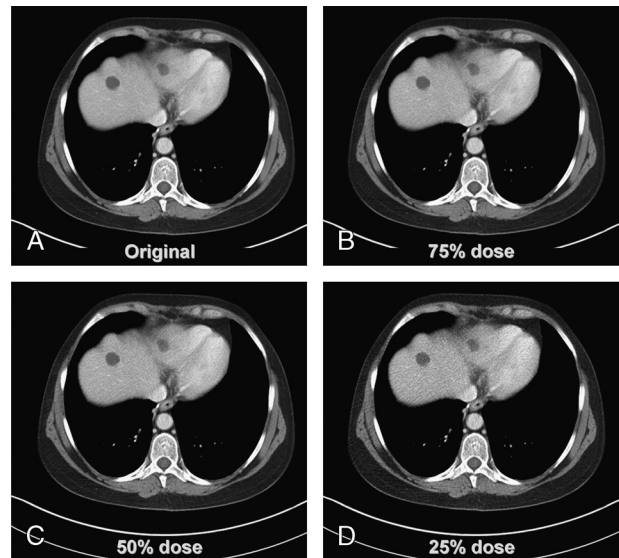


**FIGURE 11.** An example of lower-dose simulation generated from a standard-dose adult chest/abdomen/pelvis examination. Original dose (A), 75% dose (B), 50% dose (C), 25% dose (D). The original dose level corresponds to a QRM of 240. Display window/level = 400/40 HU.

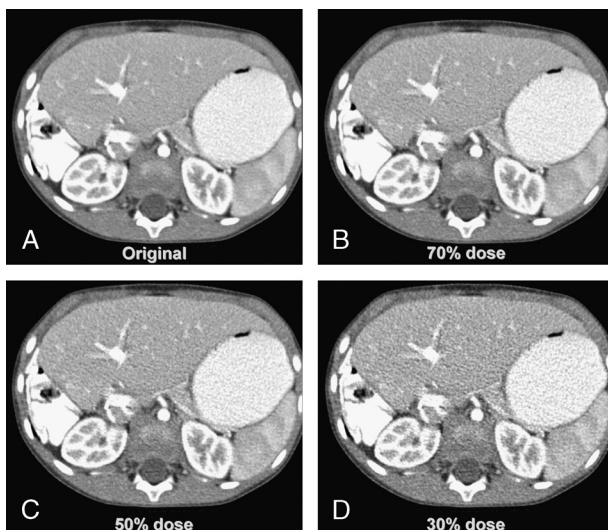


**FIGURE 12.** An example of lower-dose simulation generated from a standard-dose pediatric abdominal examination. Original dose (A), 70% dose (B), 50% dose (C), 30% dose (D). The original dose level corresponds to a QRM of 50. Display window/level = 400/40 HU.

noise insertion tools are not fully described in the literature, mostly because of the proprietary nature of the raw CT data format. The method briefly described in the study of Frush et al<sup>12</sup> and in a patent issued by General Electric<sup>26</sup> does not appear to include the important effects of the bowtie filter and AEC. In a more recent article, Massoumzadeh et al<sup>27</sup> proposed to use the compound Poisson noise model to characterize noise and to simulate reduced-dose images. Similar to their method, we also incorporated the effect of the bowtie filter, AEC, and electronic noise into the noise model. The difference is that our noise insertion method uses a relatively simpler photon-counting noise model, which is proved to be adequate in both phantom and patient studies. In addition, we proposed a unique method to incorporate the effect of electronic noise, which is calibrated by directly comparing the noise level in the simulated images with that in the acquired images at lower dose levels. We performed an extensive validation of the method, including both phantom and patient studies, and comparing both noise levels and noise spatial correlation with NPS. We have applied this tool in several different clinical areas to optimize CT scan protocols, including pediatric body and head,<sup>25,28</sup> adult abdomen,<sup>29</sup> interventional,<sup>30</sup> and brain perfusion.<sup>31</sup> A typical dose reduction is around 25% to

50% compared with our clinical routine protocols. Therefore, the accuracy of the developed tool is sufficient for most of the clinical need for optimizing CT scanning protocols.

One major difficulty of simulating very-low-dose examinations is photon starvation artifacts. These artifacts (eg, ripples or rings in the central region of the image, streaking in the shoulder region) occur when the dose level is too low for the scanned patient size, and the detected number of photons approaches the electronic noise floor in the acquired image. In this situation, the inclusion of electronic noise in a simple form like Eq. (11) may become insufficient. First, CT manufacturers usually introduce nonlinear filters on the measured data when the detected signal is low to reduce the streaking artifacts in non-uniformly attenuated regions such as the shoulder.<sup>21,32</sup> To accurately simulate the noise properties in this situation, one must have access to the raw data prior to the nonlinear filtering, which is not usually available, and have knowledge of the manufacturer's filtering algorithm. Figure 13 compares an acquired image and a simulated image at a very low dose level (80 kV, 25% of the original dose, volume CT dose index [CTDI<sub>vol</sub>] was 1.0 mGy) for an anthropomorphic phantom. One can see that, although the streaking artifacts in the shoulder region were simulated quite well, the simulated streaking has a sharper appearance than in the actually acquired image, which is probably due to the smoothing effect of the nonlinear filter.<sup>32</sup> Second, the photon starvation artifacts caused by very low dose and high attenuation are quite complicated. The proposed method does not appear to be able to simulate images at extremely low doses. Figure 14 compares the acquired and simulated images at the level of the abdomen for the same anthropomorphic phantom as in Figure 13. One can see that, with this extremely low dose level (CTDI<sub>vol</sub> = 1 mGy) for the size of the phantom (29 cm in lateral width), the severe photon starvation artifacts appearing in the actually acquired image are not accurately simulated, despite the similar noise level. Because of these 2 reasons, noise insertion tool should be used cautiously when the simulated dose level is too low that could result in severe photon starvation artifacts. However, in our validation study using the anthropomorphic phantom, we simulated lower-dose levels as low as 12.5% of the standard dose level (ie, the dose level used clinically) and still achieved accuracy within 2.1%.

We incorporated the effect of bowtie filter by calculating the noise-equivalent quanta across the x-ray beam from an air scan. It should be noted that the shape of the bowtie filter not only impacts the x-ray intensity across the beam, but also introduces a channel-dependent x-ray spectral change. The x-ray spectrum becomes harder toward the peripheral region of the beam, where the attenuation of the bowtie filter is higher. With the assumption of a photon-counting Poisson model used in this work, the effect of channel-dependent spectral change is not

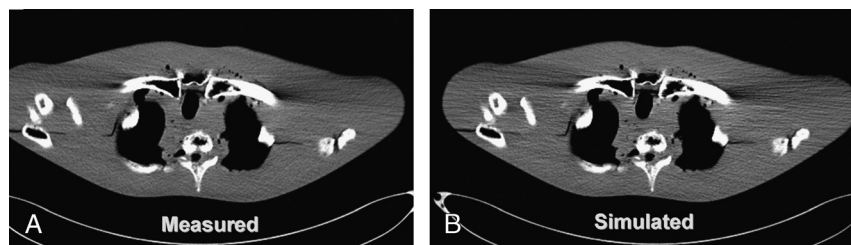


**FIGURE 13.** An example showing that the streaking artifacts caused by the high attenuation in the shoulder region can be simulated quite well using the proposed noise insertion tool. The dose level was very low (80 kV, 25% of the original dose, CTDI<sub>vol</sub> = 1.0 mGy). However, the simulated streakings have a sharper appearance than those in the actually acquired image at the same dose, which is probably due to the smoothing effect of the nonlinear filter in the preprocessing.

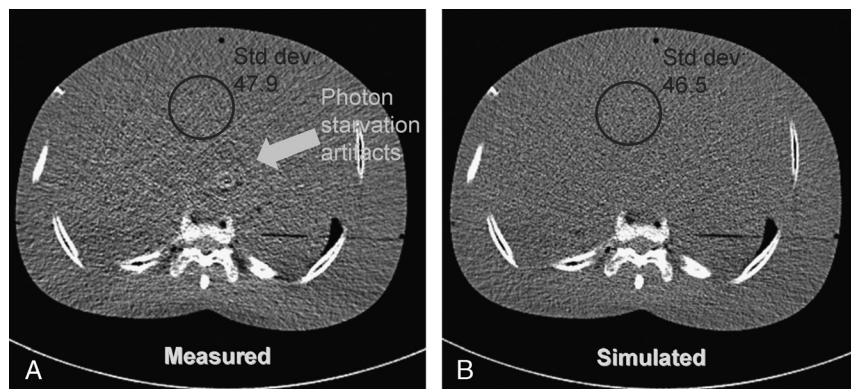


**FIGURE 14.** An example showing that photon starvation artifacts created at very low dose cannot be accurately simulated using the proposed noise insertion tool. A, An acquired image at 25% of the original dose (80 kV, CTDI<sub>vol</sub> = 1.0 mGy) and (B) a simulated image at 25% dose (80 kV, CTDI<sub>vol</sub> = 1.0 mGy).

completely incorporated. Although the results shown in Figure 4 and Table 1 demonstrated that quantifying the noise-equivalent quanta across the x-ray beam from an air scan appears to be a reasonable approximation, a full consideration of the spectral change due to bowtie filter in a noise insertion tool desires more detailed investigation.

The noise insertion tool presented here was implemented on CT scanners manufactured by Siemens Healthcare, but the general methodology is applicable to all scanners. The tool requires calibration for different scanner models and scanning modes, or when different bowtie filters or tube potentials are used. The calibration curve (noise-equivalent quanta versus detector bins at a given mAs in air) for each scanning mode is saved in a data library to allow use of the tool for a variety of scan protocols. However, the tool still requires access to the raw CT data, which unfortunately is still difficult to achieve. Numerous investigators in the field have called for manufacturers to provide access to raw data not only for purposes such as described here, but also to allow test noise reduction and iterative reconstruction algorithms developed by academic researchers.<sup>33</sup> A potential solution to this issue is for all CT manufacturers to provide a program interface that allows users to obtain raw data in a standardized format and to write raw data back to the proprietary format for reconstruction by the commercial system. With such a program and a noise insertion tool such as described here, academic and clinical researchers alike will be able to evaluate the diagnostic performance of reduced-dose scanning techniques to optimize scanning protocols in a time- and resource-efficient manner.

In conclusion, a practical technique for simulating lower-dose CT images from existing projection data acquired with a standard dose level has been developed. The technique incorporates the effect of bowtie filter, AEC, and electronic noise. Validation studies using both phantom and patient cases showed the simulation to be accurate in terms of noise level and spatial frequency information. This tool can be used to retrospectively optimize CT scanning techniques for specific diagnostic tasks.

#### ACKNOWLEDGMENTS

The authors thank Kristina Nunez and Amy Nordstrom for their assistance with manuscript preparation and Brian Welch for his help on image reconstruction. The authors also thank Dr Karl Stierstorfer and Siemens Healthcare for their support on CT raw data access.

#### REFERENCES

- Brenner DJ, Hall EJ. Computed tomography—an increasing source of radiation exposure. *N Engl J Med.* 2007;357:2277–2284.
- AAPM CT Summit. Scan Parameter Optimization. Available at: <http://www.aapm.org/meetings/2010CTS/default.asp>. Accessed January 10, 2011.
- Hendee WR, Becker GJ, Borgstede JP, et al. Addressing overutilization in medical imaging. *Radiology.* 2010;257:240–245.
- McCollough CH, Primak AN, Braun N, et al. Strategies for reducing radiation dose in CT. *Radiol Clin North Am.* 2009;47:27–40.
- FDA Notice. Public health notification: reducing radiation risk from computed tomography for pediatric and small adult patients. 2001. Available at: <http://www.fda.gov/MedicalDevices/Safety/AlertsandNotices/PublicHealthNotifications/ucm062185.htm>. Accessed June 5, 2012.
- FDA Notice. Safety investigation of CT brain perfusion scans. 2009. Available at: <http://www.fda.gov/medicaldevices/safety/alertsandnotices/ucm185898.htm>. Accessed June 5, 2012.
- Singh S, Kalra MK, Moore MA, et al. Dose reduction and compliance with pediatric CT protocols adapted to patient size, clinical indication, and number of prior studies. *Radiology.* 2009;252:200–208.
- Karmazyn B, Brush DP, Applegate KE, et al. CT with a computer-simulated dose reduction technique for detection of pediatric nephroureterolithiasis: comparison of standard and reduced radiation doses. *Am J Roentgenol.* 2009;192:143–149.
- Guimaraes LS, Fletcher JG, Harmsen WS, et al. Appropriate patient selection at abdominal dual-energy CT using 80 kV: relationship between patient size, image noise, and image quality. *Radiology.* 2010;257:732–742.
- Mayo JR, Whittall KP, Leung AN, et al. Simulated dose reduction in conventional chest CT: validation study. *Radiology.* 1997;202:453–457.
- van Gelder RE, Venema HW, Serlie IW, et al. CT colonography at different radiation dose levels: feasibility of dose reduction. *Radiology.* 2002;224:25–33.
- Brush DP, Slack CC, Hollingsworth CL, et al. Computer-simulated radiation dose reduction for abdominal multidetector CT of pediatric patients. *Am J Roentgenol.* 2002;179:1107–1113.
- Ciaschini MW, Remer EM, Baker ME, et al. Urinary calculi: radiation dose reduction of 50% and 75% at CT—effect on sensitivity. *Radiology.* 2009;251:105–111.
- Hsieh J. *Computed Tomography: Principles, Design, Artifacts, and Recent Advances.* Bellingham, WA: SPIE Press; 2006.

15. Barrett HH, Swindell W. *Radiological Imaging: The Theory of Image Formation, Detection, and Processing. Revised Edition*. Academic Press; 1981.
16. Li T, Li X, Wang J, et al. Nonlinear sinogram smoothing for low-dose x-ray CT. *IEEE Trans Nucl Sci*. 2004;51:2505–2513.
17. Wang J, Li T, Lu H, et al. Penalized weighted least-squares approach to sinogram noise reduction and image reconstruction for low-dose x-ray computed tomography. *IEEE Trans Med Imaging*. 2006;25:1272–1283.
18. Thibault JB, Sauer KD, Bouman CA, et al. A three-dimensional statistical approach to improved image quality for multislice helical CT. *Med Phys*. 2007;34:4526–4544.
19. Manduca A, Yu L, Trzasko JD, et al. Projection space denoising with bilateral filtering and CT noise modeling for dose reduction in CT. *Med Phys*. 2009;36:4911–4919.
20. Whiting BR, Massoumzadeh P, Earl OA, et al. Properties of preprocessed sinogram data in x-ray computed tomography. *Med Phys*. 2006;33:3290–3303.
21. Hsieh J. Adaptive streak artifact reduction in computed tomography resulting from excessive x-ray photon noise. *Med Phys*. 1998;25:2139–2147.
22. Siewersen JH, Cunningham IA, Jaffray DA. A framework for noise-power spectrum analysis of multidimensional images. *Med Phys*. 2002;29:2655–2671.
23. Boedeker KL, Cooper VN, McNitt-Gray MF. Application of the noise power spectrum in modern diagnostic MDCT: part I. Measurement of noise power spectra and noise equivalent quanta. *Phys Med Biol*. 2007;52:4027–4046.
24. Boedeker KL, McNitt-Gray MF. Application of the noise power spectrum in modern diagnostic MDCT: part II. Noise power spectra and signal to noise. *Phys Med Biol*. 2007;52:4047–4061.
25. Yu L, Bruesewitz MR, Thomas KB, et al. Optimal tube potential for radiation dose reduction in pediatric CT: principles, clinical implementations, and pitfalls. *Radiographics*. 2011;31:835–848.
26. Toth TL, Hsieh J, Li J, et al. Method and system for low dose image simulation for imaging systems. 2004;US patent 6,829,323.
27. Massoumzadeh P, Don S, Hildebolt CF, et al. Validation of CT dose-reduction simulation. *Med Phys*. 2009;36:174–189.
28. Morris J, Delone D, Yu L, et al. Radiation dose reduction and protocol optimization for pediatric head and sinus CT using a novel low-dose simulation tool. Presented at the American Society of Neuroradiology Annual Meeting; May 16–21, 2009; Vancouver, Canada.
29. Apel A, Fletcher JG, Fidler JL, et al. Pilot multi-reader study demonstrating potential for dose reduction in dual energy hepatic CT using non-linear blending of mixed kV image datasets. *Eur Radiol*. 2011;21:644–652.
30. Leng S, Atwell TD, Yu L, et al. Radiation dose reduction for CT-guided renal tumor cryoablation. *Am J Roentgenol*. 2011;196:W586–W591.
31. Yu L, Lindell E, Delone D, et al. Radiation dose evaluation and reduction in CT brain perfusion. Presented at the 96th Scientific Assembly and Annual Meeting of the Radiological Society of North America; November 28–December 3, 2010; Chicago, IL.
32. Kachelriess M, Watzke O, Kalandar WA. Generalized multi-dimensional adaptive filtering for conventional and spiral single-slice, multi-slice, and cone-beam CT. *Med Phys*. 2001;28:475–490.
33. Pan XC, Sidky EY, Vannier M. Why do commercial CT scanners still employ traditional, filtered back-projection for image reconstruction? *Inverse Probl*. 2009;25:123009.